ADVANCED HEALTHCARE MATERIALS
www.advhealthmat.de

A Pharmacokinetic Model of a Tissue Implantable Insulin Sensor

*Gili Bisker, Nicole M. Iverson, Jiyoung Ahn, and Michael S. Strano**

While implantable sensors such as the continuous glucose monitoring system have been widely studied, both experimentally and mathematically, relatively little attention has been applied to the potential of insulin sensors. Such sensors can provide feedback control for insulin infusion systems and pumps and provide platforms for the monitoring of other biomarkers in vivo. In this work, the first pharmacokinetic model of an affinity sensor is developed for insulin operating subcutaneously in the limit of where mass transfer across biological membranes reaches a steady state. Using a physiological, compartmental model for glucose, insulin, and glucagon metabolism, the maximum sensor response and its delay time relative to plasma insulin concentration, are calculated based on sensor geometry, placement, and insulin binding parameters for a sensor localized within adipose tissue. A design relation is derived linking sensor dynamics to insulin time lag and placement within human tissue. The model should find utility in understanding dynamic insulin responses and forms the basis of model predictive control algorithms that incorporate sensor dynamics.

1. Introduction

Insulin is a 5.8 kDa naturally occurring hormone, synthesized and secreted by pancreatic β-cells, and is part of the glucose homeostasis regulation system in the body. Impaired glucose metabolism occurs in diabetes mellitus,[1] which is a metabolic disease affected by nearly 26 million people in the United States alone. Approximately 90% of diabetes cases are of type II (non-insulin-dependent), characterized by insulin resistance and partial insulin deficiency, whereas type I diabetes (insulin-dependent) is characterized by destruction of the insulin producing cells resulting in a complete insulin deficiency.[1] Patients who suffer from type I diabetes rely on various insulin drugs administered on a daily basis based on the transient glucose level.[2] Continuous glucose monitoring (CGM) along with insulin pump infusion was proven to be a better course of treatment for insulin-dependent diabetes than injection treatment, in terms of glycated hemoglobin level[3] (which correlates to the average glucose levels of the previous 2–3 months[4]), and was shown to decrease hypoglycemia events.[5] Recent technological advantages have led to an FDA-approved insulin pump that includes CGM in real time and an automated subcutaneous insulin infusion pump that stops when blood glucose levels drop below a certain threshold (MiniMed 530G, Medtronic Inc.). However, insulin levels are not monitored in real time in such automated systems and the insulin dosage is determined by a proportional-integrative-derivative (PID) control algorithm solely based on the glucose levels.[5b,6]

Continuous insulin monitoring (CIM) can accompany the PID control algorithm of the closed loop system, providing additional regulation to its control. If available, CIM can recognize patient-specific elevated insulin levels, which increase the risk of hypoglycemia in type I diabetes patients who are treated with an insulin pump. Moreover, it can be utilized for diagnosing complications. For example, fasting insulin levels can be used as a marker for insulin resistance,[7] which can occur in both type I and type II diabetes.[8] Insulin levels can also monitor progression of β-cell dysfunction in type II diabetes, and insulin response to glucose infusion in insulin-resistant patients can be used to assess their insulin sensitivity.[9]

Normal fasting concentration levels of insulin in blood range between 50 and 80 $\times$ 10^{-12} M,[10] hence requiring highly sensitive and selective detection and quantification. Insulin concentrations in blood samples were first detected by radioimmunoassay,[11] which was later replaced by an enzyme-linked immunosorbent assay.[12] Other methods include quartz crystal microbalance (QCM),[10] electrochemical impedance spectroscopy (EIS),[13] surface plasmon resonance (SPR),[14] carbon-nanotube-modified electrode,[15] and nickel-powder-modified electrode.[16] Additional approaches utilize QCM transducers and molecularly imprinted polymers either by insulin or an insulin antibody; however, the detection limit is in the mM range.[17] Alternative methods include imaging ellipsometry of an insulin antibody-modified gold surface,[18] fluorescent imaging of fluorescently labeled insulin binding aptamer

Dr. G. Bisker, J. Ahn, Prof. M. S. Strano
Department of Chemical Engineering
Massachusetts Institute of Technology
77 Massachusetts Avenue
Cambridge, MA 02139, USA
E-mail: strano@mit.edu
Dr. N. M. Iverson
Department of Biological Engineering
Massachusetts Institute of Technology
77 Massachusetts Avenue
Cambridge, MA 02139, USA

DOI: 10.1002/adhm.201400264

immobilized on graphene oxide,[19] and hyperspectral Raman spectroscopy of human islets of Langerhans.[20]

Recently, our group has presented a new concept for analyte detection utilizing the corona phase of a polymer wrapped nanoparticle for molecular recognition, CoPhMoRe.[21] Here, the polymer adopts a configuration such that recognition of a specific molecule is enabled, rendering the nanoparticle configuration a "synthetic antibody." When applied to the surface of semiconducting single-walled carbon nanotubes (SWNTs), which fluoresce in the near-infrared range, the result is a fluorescent sensor for the target analyte utilizing either the intensity change or a wavelength shift of the emission for detection.[22] Moreover, our group has recently demonstrated the feasibility of in vivo detection using a biocompatible hydrogel for SWNT sensor encapsulation and subcutaneous implantation.[23] The unique optical and electronic properties of SWNTs[24] render them favorable as in vivo fluorescent imaging agents[25] owing to their fluorescence in the near-infrared range,[26] where tissue and blood are mostly transparent,[27] and their lack of photobleaching.[28]

In this work, we present a theoretical model for designing an in vivo insulin sensor for continuous, real time, detection of insulin. The proposed sensor is based on a tailored polymer–fluorescent sensor complex capable of optically detecting insulin selectively. The sensor is encapsulated within a biocompatible hydrogel implanted in the subcutaneous adipose tissue, where its presumed near-infrared fluorescence allows for external noninvasive optical detection (**Figure 1**). Although hydrogels have been implanted in vivo in many tissue types, including bone,[29] liver,[30] pancreas,[31] kidneys,[32] muscle,[33] intestines,[34] and subcutaneous tissue,[35] the latter is the most accessible for external measurements.[23]

We use a full physiological compartmental model of glucose, insulin, and glucagon metabolism, based on the model of Sorensen.[36] This model includes 22 differential equations for describing the various compartments in the human body, including the brain, heart and lungs, gut, liver, kidney, and periphery. In order to predict insulin levels in adipose interstitial volume, where the proposed sensor would be implanted, we have divided the periphery compartment into two separate subcompartments of muscle tissue and adipose tissue, extending the model to a total of 26 coupled ordinary differential equations for the transient insulin, glucose, and glucagon concentrations. We then model insulin diffusion into the hydrogel and the response of the embedded insulin sensors, optimizing the gel, sensor, and interaction parameters for optimal insulin in vivo detection.

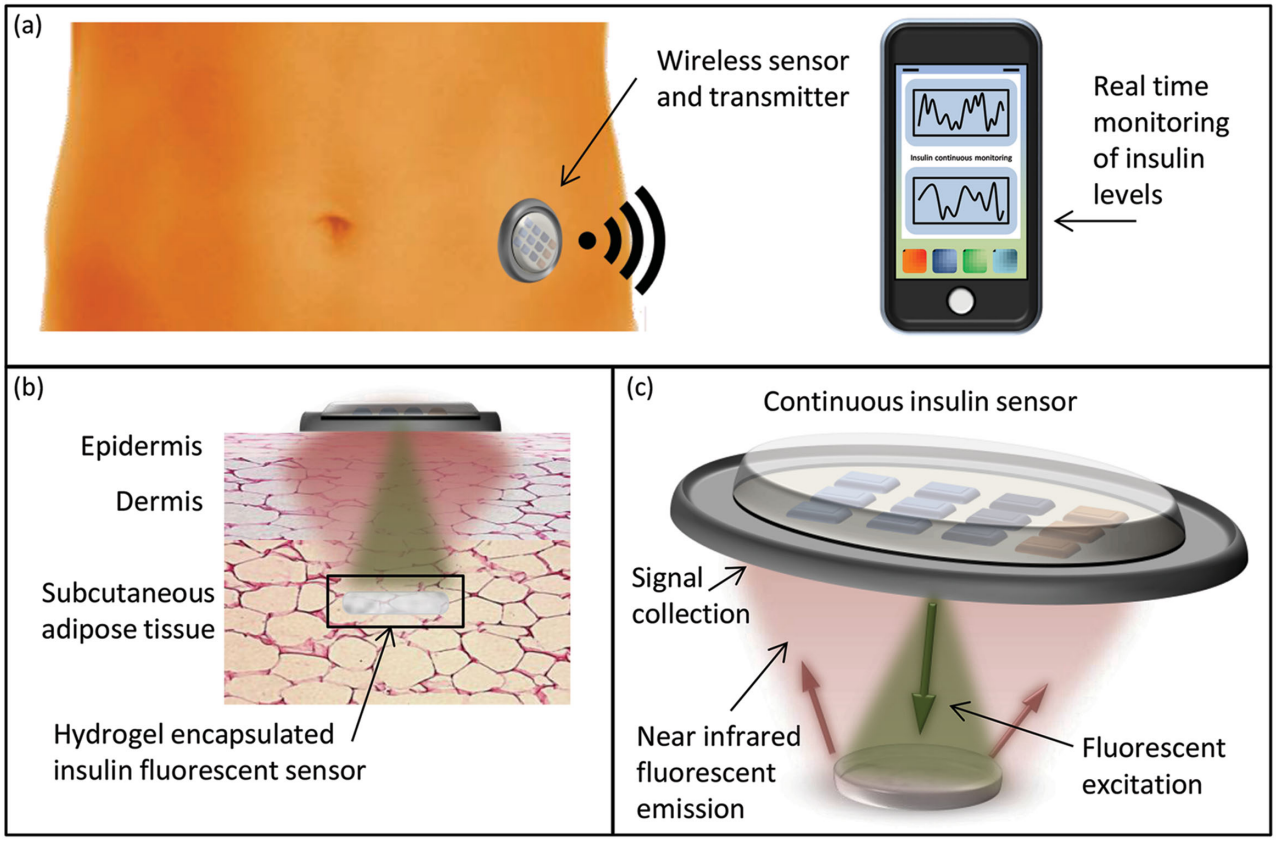

Figure 1. Illustration of a prototypical optical sensor for insulin implanted in the interstitial subcutaneous adipose tissue. a) The detection consists of a near-infrared fluorescent sensor encapsulated in a hydrogel that is implanted within adipose tissue along with a dermal patch providing optical excitation and collection through the interposed tissue with detection read telemetrically. b) The sensor is placed at a fixed depth into subcutaneous adipose tissue where c) the external dermal patch provides optical excitation through the tissue, querying the sensor for insulin concentration, and receiving a proportional emission signal back through the tissue for collection at the patch.

2. Theoretical Basis

The insulin metabolism cannot be decoupled from the glucose and glucagon concentrations in the body. For example, the glucose uptake in the periphery interstitial volume as well as in the liver is regulated by the local insulin concentration. Moreover, hepatic glucose production is regulated by both the local insulin and glucagon concentrations, and the pancreas insulin release is regulated by glucose blood levels. Therefore, a complete physiological model requires consideration of all transient concentrations of glucose, insulin, and glucagon.

Our analysis follows that of Sorensen[36] by dividing the human body into isochoric compartments, including the capillary volume and the interstitial volume, and allowing for the solute to flow into and out of each compartment with mass transport between them. The solute convectively travels from the arterial blood to the capillary volume V_C, with rate Q_C, from which it can diffuse to the interstitial volume V_S with characteristic transcapillary diffusion time T. Moreover, metabolic sources and sinks can give rise to additional accumulation or depletion of the solute. The mass balance can be written as follows:

$$V_C \frac{dC_{CB}}{dt} = Q_C (C_{AB} - C_{CB}) + \frac{V_S}{T}(C_S - C_{CB}) - r_{RBCU} \quad (1)$$

and

$$V_S \frac{dC_S}{dt} = \frac{V_S}{T}(C_{CB} - C_S) - r_T \quad (2)$$

where C_{AB}, C_{CB}, and C_S are the solute concentrations in the arterial blood, capillary blood, and the interstitial fluid respectively, and r_{RBCU} and r_T are the rates of solute uptake by red blood cells and the tissue, respectively. Rapid transcapillary diffusion allows for the capillary and interstitial volumes to be considered as one compartment and to be described by a single equation. This is the case for the heart and lungs, liver, gut, and kidney in both the glucose and insulin subsystems.[36] The brain and periphery compartments are divided into the capillary volume and the interstitial volume and are described by two equations similar to Equation (1) and (2), with the exception of the brain cerebrospinal fluid, which is impermeable to insulin and thus omitted from the equations.[36] Compared to glucose, which is a small molecule that can exhibit rapid blood clearance,[37] insulin is a small peptide that is presumably less permeable by the capillary wall. However, past studies have shown that the capillaries in the liver, kidney, and gut are more permeable to insulin than in the periphery, confirming that each of those organs can be combined into a single compartment in the model.[36]

Our compartmental model, in which we have modified the original Sorensen model by dividing the periphery compartment into muscle and adipose tissue, is illustrated in **Figure 2**. The variables in this model are summarized in **Table 1**.

The corresponding new variables must obey the following relations for both the glucose and insulin subsystems:

$$\begin{aligned} V_{MP} + V_{AP} &= V_P \\ Q_{MP} + Q_{AP} &= Q_P \end{aligned} \quad (3)$$

where the ratio between the corresponding blood flow rate was estimated using the work of Mapleson,[38] who considered blood flow rates in the various body compartments for modeling the distribution of inhaled inert gases:

$$\frac{Q_{MP}}{Q_{AP}} = 2.5 \quad (4)$$

2.1. Glucose System

The new equations for the vascular and interstitial compartments of muscle and adipose tissue, respectively, in the glucose system are:

$$\begin{aligned} V^G_{MPV} \frac{dG_{MPV}}{dt} &= Q^G_{MP}(G_H - G_{MPV}) - \frac{V^G_{MPI}}{T^G_{MP}}(G_{MPV} - G_{MPI}) \\ V^G_{MPI} \frac{dG_{MPI}}{dt} &= \frac{V^G_{MPI}}{T^G_{MP}}(G_{MPV} - G_{MPI}) - r_{MPGU} \\ V^G_{APV} \frac{dG_{APV}}{dt} &= Q^G_{AP}(G_H - G_{APV}) - \frac{V^G_{API}}{T^G_{AP}}(G_{APV} - G_{API}) \\ V^G_{API} \frac{dG_{API}}{dt} &= \frac{V^G_{API}}{T^G_{AP}}(G_{APV} - G_{API}) - r_{APGU} \end{aligned} \quad (5)$$

The relations to the original parameters in the Sorensen model are:

$$\begin{aligned} V^G_{MPV} G_{MPV} + V^G_{APV} G_{APV} &= V^G_{PV} G_{PV} \\ V^G_{MPI} G_{MPI} + V^G_{API} G_{API} &= V^G_{PI} G_{PI} \end{aligned} \quad (6)$$

and:

$$r_{MPGU} + r_{APGU} = r_{PGU} \quad (7)$$

where muscle and adipose tissues are responsible for 89% and 11% of the total periphery glucose uptake,[39] r_{PGU}, respectively, so $r_{MPGU} = 0.89 \times r_{PGU}$ and $r_{APGU} = 0.11 \times r_{PGU}$. Estimation of the corresponding volumes and blood flows in the vascular blood volume was performed using the relations in Equations (3) and (4), and by assuming:

$$\frac{V^G_{MPV}}{Q^G_{MP}} = \frac{V^G_{APV}}{Q^G_{AP}} = \frac{V^G_{PV}}{Q^G_P} \quad (8)$$

where V^G_{PV} and Q^G_P are parameters of the original Sorensen model. For the interstitial volume we assume:

$$\frac{V^G_{MPI}}{V^G_{MPV}} = \frac{V^G_{API}}{V^G_{APV}} = \frac{V^G_{PI}}{V^G_{PV}} \quad (9)$$

and set:

$$T^G_{MP} = T^G_{AP} = T^G_P \quad (10)$$

where V^G_{PI} and T^G_P are parameters of the original Sorensen model.

Finally, the equation for the heart and lungs, which closes the circulatory blood loop, becomes:

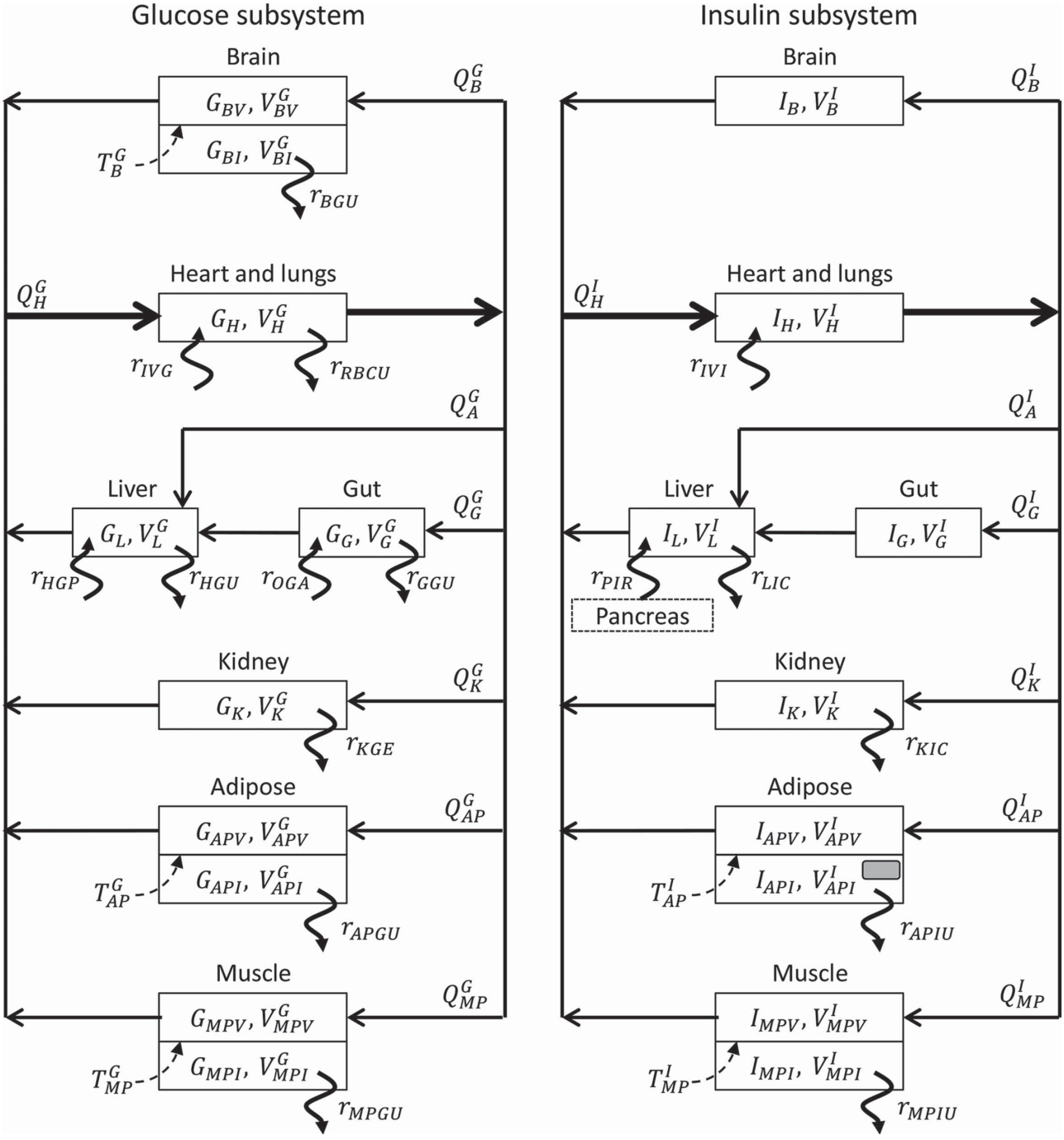

Figure 2. Compartmental model for glucose (left) and insulin (right) metabolism. The heart and lung compartment represents the cardiopulmonary blood and the major arteries and drain the entire circulatory loop. The arterial blood feeds the capillaries in the gut, liver, kidney, peripheral adipose and muscle tissues, while the liver also receives blood from the hepatic portal vein originating in the gut. The brain in the glucose subsystem and the peripheral adipose and muscle tissues in both the glucose and insulin subsystems are divided into capillary and interstitial volumes to account for longer transcapillary diffusion times. The insulin sensor represented by a gray rectangle is embedded within the peripheral interstitial adipose volume. See Table 1 for an explanation of each variable.

$$V_H^G \frac{dG_H}{dt} = Q_B^G G_{BV} + Q_L^G G_L + Q_K^G G_K + \left(Q_{MP}^G G_{MPV} + Q_{AP}^G G_{APV}\right) - Q_H^G G_H - r_{RBCU} + r_{IVG} \quad (11)$$

2.2. Insulin System

The new equations for the vascular and interstitial compartments of the muscle and adipose tissue, respectively, in the insulin system are:

Table 1. Variables in the modified model.

Variables		Metabolic rates subscripts	
G	Glucose concentration	BGU	Brain glucose uptake
I	Insulin concentration	RBCU	Red blood cells glucose uptake
Q	Vascular blood flow rate	GGU	Gut glucose utilization
V	Volume	HGU	Hepatic glucose uptake
r	Metabolic source or sink rate	KGE	Kidney glucose excretion
T	Transcapillary diffusion time	APGU	Adipose peripheral glucose uptake
t	Time	MPGU	Muscle peripheral glucose uptake
Compartment – first subscript		IVG	Intravenous glucose infusion
B	Brain	OGA	Gut oral glucose absorption
H	Heart and lungs	HGP	Hepatic glucose production
G	Gut	LIC	Liver insulin clearance
L	Liver	KIC	Kidney insulin clearance
K	Kidney	APIU	Adipose peripheral insulin uptake
P	Periphery	MPIU	Muscle peripheral insulin uptake
AP	Adipose periphery	IVI	Intravenous insulin infusion
MP	Muscle periphery	PIR	Pancreatic insulin release
A	Hepatic artery		
Subcompartment – second subscript		Model – superscript	
I	Interstitial fluid	G	Glucose
V	Vascular blood	I	Insulin

$$\begin{aligned}
V^I_{\mathrm{MPV}}\frac{\mathrm{d}I_{\mathrm{MPV}}}{\mathrm{d}t} &= Q^I_{\mathrm{MP}}\left(I_{\mathrm{H}}-I_{\mathrm{MPV}}\right)-\frac{V^I_{\mathrm{MPI}}}{T^I_{\mathrm{MP}}}\left(I_{\mathrm{MPV}}-I_{\mathrm{MPI}}\right)\\
V^I_{\mathrm{MPI}}\frac{\mathrm{d}I_{\mathrm{MPI}}}{\mathrm{d}t} &= \frac{V^I_{\mathrm{MPI}}}{T^I_{\mathrm{MP}}}\left(I_{\mathrm{MPV}}-I_{\mathrm{MPI}}\right)-r_{\mathrm{MPIC}}\\
V^I_{\mathrm{APV}}\frac{\mathrm{d}I_{\mathrm{APV}}}{\mathrm{d}t} &= Q^I_{\mathrm{AP}}\left(I_{H}-I_{\mathrm{APV}}\right)-\frac{V^I_{\mathrm{API}}}{T^I_{\mathrm{AP}}}\left(I_{\mathrm{APV}}-I_{\mathrm{API}}\right)\\
V^I_{\mathrm{API}}\frac{\mathrm{d}I_{\mathrm{API}}}{\mathrm{d}t} &= \frac{V^I_{\mathrm{API}}}{T^I_{\mathrm{AP}}}\left(I_{\mathrm{APV}}-I_{\mathrm{API}}\right)-r_{\mathrm{APIC}}
\end{aligned} \tag{12}$$

and the equation for the heart and lungs becomes:

$$\begin{aligned}
V^I_H\frac{\mathrm{d}I_H}{\mathrm{d}t} &= Q^I_B I_B+Q^I_L I_L+Q^I_K I_K\\
&\quad+\left(Q^I_{\mathrm{MP}}I_{\mathrm{MPV}}+Q^I_{\mathrm{AP}}I_{\mathrm{APV}}\right)-Q^I_H I_H+r_{\mathrm{IVI}}
\end{aligned} \tag{13}$$

The relations to the original parameters in the Sorensen model are:

$$\begin{aligned}
V^I_{\mathrm{MPV}}I_{\mathrm{MPV}}+V^I_{\mathrm{APV}}I_{\mathrm{APV}} &= V^I_{\mathrm{PV}}I_{\mathrm{PV}}\\
V^I_{\mathrm{MPI}}I_{\mathrm{MPI}}+V^I_{\mathrm{API}}I_{\mathrm{API}} &= V^I_{\mathrm{PI}}I_{\mathrm{PI}}
\end{aligned} \tag{14}$$

and

$$r_{\mathrm{MPIC}}+r_{\mathrm{APIC}}=r_{\mathrm{PIC}} \tag{15}$$

Since the peripheral insulin uptake rate, r_{PIC}, is linearly proportional to the peripheral vascular blood flow rate, we assume:

$$\begin{aligned}
r_{\mathrm{MPIC}} &= \frac{Q^I_{\mathrm{MP}}}{Q^I_P}r_{\mathrm{PIC}}\\
r_{\mathrm{APIC}} &= \frac{Q^I_{\mathrm{AP}}}{Q^I_P}r_{\mathrm{PIC}}
\end{aligned} \tag{16}$$

Similar to the glucose system, we set:

$$T^I_{\mathrm{MP}}=T^I_{\mathrm{AP}}=T^I_P \tag{17}$$

The parameter values for a 70 kg man[36] and the complete set of equations can be found in the Supporting Information. For the glucose model, since the water content of blood is about 84%, its corresponding volumes are decreased by 16% from the total vascular volume.[36] For the insulin model, since the average red blood cell volume content of whole blood is about 40%, the blood volumes as estimated for a 70 kg man were decreased by 40% from the total vascular volume.[36]

2.3. Meal Absorption

Following the model of Lehmann and Deutsch,[40] the oral glucose absorption rate by the gut, r_{OGA}, was assumed to linearly increase up to a maximal gastric emptying rate,[36] $V_{\max}=800\ \mathrm{mg\,min^{-1}}$, during a time period of T_{inc} minutes, remain constant for $T_{\max}$ minutes, and then linearly decrease to zero during a time period of T_{dec} minutes. For a meal of M_g grams of glucose, the duration of maximal absorption rate is:

$$T_{\max} = \mathrm{Max}\left\{\frac{M_g}{V_{\max}} - \frac{1}{2}(T_{\mathrm{inc}} + T_{\mathrm{dec}}), 0\right\} \tag{18}$$

where $T_{\mathrm{inc}} = 10\,\mathrm{min}$, $T_{\mathrm{dec}} = 60\,\mathrm{min}$, and $\mathrm{Max}\{.,.\}$ refers to the maximal value between the two input variables. When $T_{\max} > 0$ the oral glucose absorption rate for a meal eaten in time t_0 is:

$$\begin{aligned} r_{\mathrm{OGA}} &= V_{\max}\frac{t-t_0}{T_{\mathrm{inc}}}\left[H(t-t_0) - H(t-t_0-T_{\mathrm{inc}})\right] + \\ &+ V_{\max}\left[H(t-t_0-T_{\mathrm{inc}}) - H(t-t_0-T_{\mathrm{inc}}-T_{\max})\right] + \\ &+ V_{\max}\left(1 - \frac{t-t_0-T_{\mathrm{inc}}-T_{\max}}{T_{\mathrm{dic}}}\right)\left[H(t-t_0-T_{\mathrm{inc}}-T_{\max})\right. \\ &\left. - H(t-t_0-T_{\mathrm{inc}}-T_{\max}-T_{\mathrm{dic}})\right] \end{aligned} \tag{19}$$

where $H(t)$ is the Heaviside step function at t.

When $T_{\max} = 0$ we assume:

$$\begin{aligned} r_{\mathrm{OGA}} &= V'_{\max}\frac{t-t_0}{T'_{\mathrm{inc}}}\left[H(t-t_0) - H\left(t-t_0-T'_{\mathrm{inc}}\right)\right] + \\ &+ V'_{\max}\left(1 - \frac{t-t_0-T'_{\mathrm{inc}}}{T'_{\mathrm{dic}}}\right)\left[H\left(t-t_0-T'_{\mathrm{inc}}\right)\right. \\ &\left. - H\left(t-t_0-T'_{\mathrm{inc}}-T'_{\mathrm{dic}}\right)\right] \end{aligned} \tag{20}$$

where $T'_{\mathrm{inc}} : T'_{\mathrm{dec}} = 1:6$, and

$$\frac{T'_{\mathrm{inc}}}{T_{\mathrm{inc}}} = \frac{T'_{\mathrm{dec}}}{T_{\mathrm{dec}}} = \frac{V'_{\max}}{V_{\max}} \tag{21}$$

such that

$$\frac{1}{2}\left(T'_{\mathrm{inc}} + T'_{\mathrm{dec}}\right)V'_{\max} = M_g \tag{22}$$

See **Figure 3** for illustration of the oral glucose absorption rate by the gut for different scenarios.

2.4. Insulin Sensor Kinetics

We assume a sensor completely specific to insulin, such as a hypothetical corona phase of a specifically functionalized near-infrared fluorescent SWNT for molecular recognition[21a] of insulin. We model the insulin–sensor association by second-order kinetics:

$$C_I + \theta \underset{k_{-1}}{\overset{k}{\rightleftarrows}} \overline{C_I\theta} \tag{23}$$

Where C_I is the free insulin concentration in the vicinity of the sensor, θ is an unoccupied binding site on the sensor, $\overline{C_I\theta}$ is the site bound insulin, and k and k_{-1} are the forward and reverse rate constants, respectively. The total binding site concentration θ_T, which remains constant, is given by:

$$\theta_T = [\theta] + \left[\overline{C_I\theta}\right] \tag{24}$$

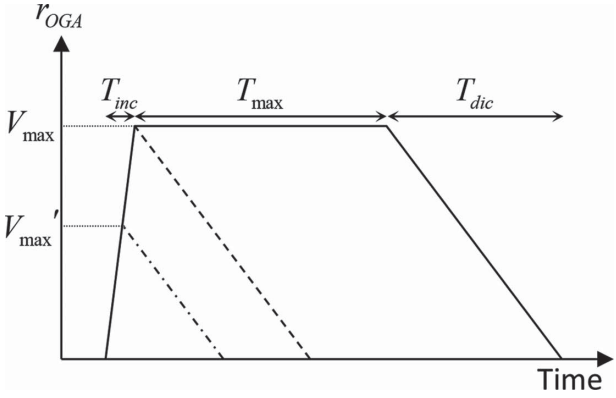

Figure 3. Oral glucose absorption rate by the gut for $T_{\max} > 0$ (solid line), for $V'_{\max} = V_{\max}$ (dashed line) and for $V'_{\max} < V_{\max}$ (dashed-dotted line).

where the brackets represent concentrations of the respective entities.

Using the dissociation constant:

$$K_d = \frac{k_{-1}}{k} = \frac{[C_I][\theta]}{\left[\overline{C_I\theta}\right]} \tag{25}$$

the reaction rate is:

$$\begin{aligned} r &= -\frac{\mathrm{d}[C_I]}{\mathrm{d}t} = k[C_I][\theta] - kK_{\mathrm{d}}\left[\overline{C_I\theta}\right] \\ &= k[C_I][\theta] - kK_d\left(\theta_T - [\theta]\right) \end{aligned} \tag{26}$$

and

$$\frac{\mathrm{d}\left[\overline{C_I\theta}\right]}{\mathrm{d}t} = -\frac{\mathrm{d}[C_I]}{\mathrm{d}t} = -\frac{\mathrm{d}[\theta]}{\mathrm{d}t} \tag{27}$$

The sensor fluorescence response is assumed to be linearly proportional[21a] to the relative sensor surface coverage by insulin molecules with the proportion factor β:

$$\frac{F - F_0}{F_0} = -\beta\frac{\left[\overline{C_I\theta}\right]}{\theta_T} \tag{28}$$

where F is the measured fluorescence intensity in the presence of insulin, and F_0 is the initial intensity.

2.5. Hydrogel Diffusion

We assume a sensor encapsulated within a biocompatible hydrogel[23] and implanted in the subcutaneous adipose tissue for continuous insulin monitoring. The hydrogel is modeled as a thin disk such that its diameter is much larger than its thickness, allowing one to neglect diffusion in the radial direction, and only account for 1D diffusion across the gel.[41] The insulin concentration within the hydrogel follows the nonhomogeneous diffusion equation:

$$\frac{\partial C_I^h}{\partial t} = D\frac{\partial^2 C_I^h}{\partial x^2} + r \tag{29}$$

where C_I^h is the insulin concentration within the hydrogel, r is the sensor–insulin reaction rate, and D is the diffusion coefficient. The boundary condition for the hydrogel is the transient insulin concentration within the interstitial adipose tissue, I_{API}, and the initial condition is taken to be the basal insulin level in that subcompartment, according to our model.

We define a dimensionless length scale:

$$z = \frac{x}{L} \tag{30}$$

where L is the thickness of the gel, and a dimensionless time scale:

$$\tau = \frac{t}{\tau_D} \tag{31}$$

where τ_D is the characteristic diffusion time:

$$\tau_D = \frac{L^2}{D} \tag{32}$$

The characteristic reaction time of the sensor is then given by:

$$\tau_R = \frac{1}{k\theta_T} \tag{33}$$

and the Thiele modulus is defined as:

$$\phi \equiv \frac{\tau_D}{\tau_R} = \frac{k\theta_T L^2}{D} \tag{34}$$

Using the dimensionless concentration

$$g = \frac{[\theta]}{\theta_T} \tag{35}$$

Equation (26), (27) and (29) can be combined to:

$$\frac{\partial C_I^h}{\partial \tau} = \frac{\partial^2 C_I^h}{\partial z^2} - \phi\left[gC_I^h + K_d\left(1-g\right)\right] \tag{36}$$

and

$$\frac{\mathrm{d}g}{\mathrm{d}\tau} = -\frac{\phi}{\theta_T}\left[gC_I^h - K_d\left(1-g\right)\right] \tag{37}$$

where the sensor response is:

$$\frac{F-F_0}{F_0} = -\beta\left(1-g\right) \tag{38}$$

The schematics and parameters of the insulin sensor model are visualized in **Figure 4**.

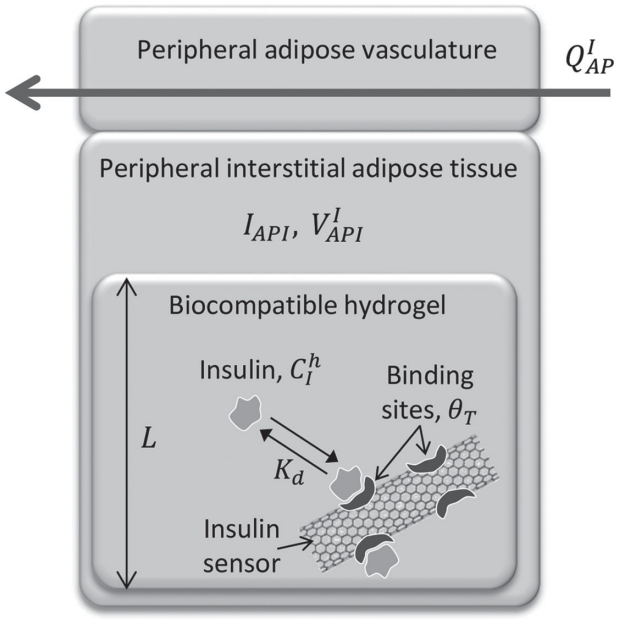

Figure 4. Implantable insulin sensor schematic. Blood flows in the peripheral adipose vasculature with rate Q_{AP}^I from which insulin diffuses into the interstitial tissue of volume V_{API}^I resulting in transient insulin concentration of I_{API} within this volume. Insulin diffuses into the hydrogel of thickness L, resulting in transient insulin concentration of C_I^h within the gel. Insulin sensors are dispersed throughout, having total insulin binding site concentration of θ_T, and encapsulated in the hydrogel, where insulin is in equilibrium between free and bound state with a dissociation constant K_d.

3. Results and Discussion

3.1. Insulin and Glucose Dynamics

The glucose and insulin levels in the various body compartments, and the normalized glucagon levels, following a meal of 100 g of glucose at $t = 0$ are presented in **Figure 5**.

The blood glucose and insulin concentrations in the peripheral adipose vasculature peak after 88 and 115 min, respectively (Figure 5, panels (i) and (r)), following the beginning of the meal, whereas the interstitial peak concentrations lag by 3 and 7 min, respectively (Figure 5, panels (j) and (s)), in agreement with previous findings.[42] By fitting an exponential function to the peripheral adipose interstice insulin concentration, a characteristic time for tissue insulin response was found to be $\tau_{\mathrm{tissue}} = 57$ min.

3.2. Insulin Sensor Response

We evaluate the dissociation constant of insulin to SWNT by its dissociation constant of adsorption onto a hydrophobic surface[43] $K_d = 8.3\ \mu\mathrm{M}$, which is comparable to other SWNT-based sensors,[21a] and the rate constant from the kinetics of anti-insulin antibody binding to insulin[44] $k = 1\times10^5\ \mathrm{M^{-1}s^{-1}}$. The total binding sites concentration was calculated by assessing a 10 mg $\mathrm{L^{-1}}$ SWNT concentration within the hydrogel, an average nanotube length of 1 μm, and assuming an insulin binding site every 50 nm.[28] The diffusion coefficient of insulin within

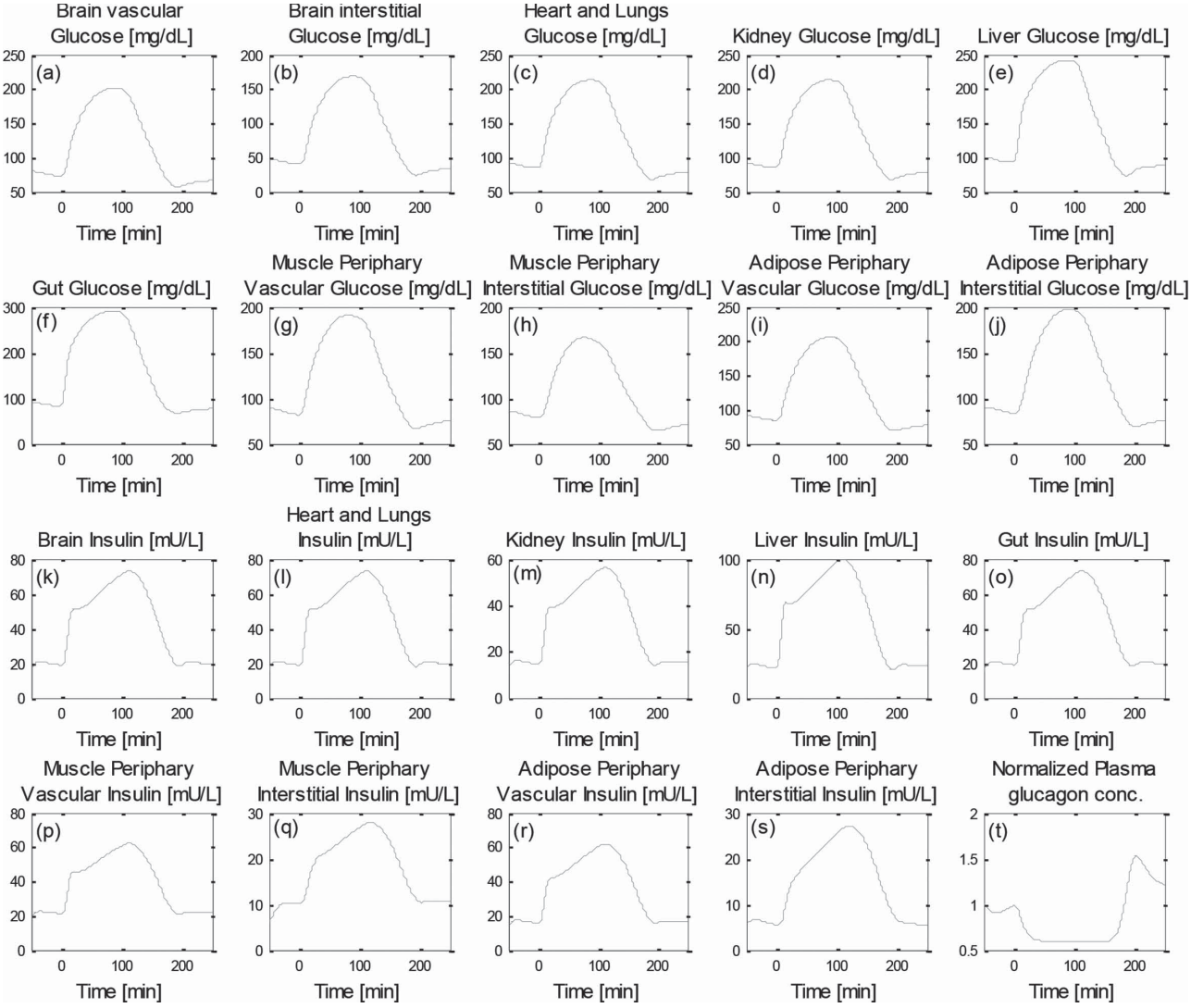

Figure 5. Glucose, insulin and glucagon concentrations in the various body compartments following a 100 g glucose meal at $t = 0$ according to our model. a–j) Glucose concentration in a) Brain vasculature, b) Brain interstice, c) Heart and lungs, d) Kidney, e) Liver, f) Gut, g) Muscle periphery vasculature, h) Muscle periphery interstice, i) Adipose periphery vasculature, and j) Adipose periphery interstice. k–s) Insulin concentration in k) Brain, l) Heart and lungs, m) Kidney, n) Liver, o) Gut, p) Muscle periphery vasculature, q) Muscle periphery interstice, r) Adipose periphery vasculature, and s) Adipose periphery interstice. t) Normalized glucagon concentration in plasma.

the hydrogel was estimated by $D = 10^{-6}\,\mathrm{cm^2 s^{-1}}$, based on experimental results.[41] Choosing a gel thickness of $L = 0.5$ mm, this set of parameters yields:

$$\tau_D = 2.5 \times 10^3\, s \tag{39}$$

and

$$\tau_R = 50\ s \tag{40}$$

assuring that $\tau_R \le \tau_D \le \tau_{\mathrm{tissue}}$ so that the limiting factor would not results from the sensor encapsulation or the sensor reaction.

The diffusion profile of the insulin into the hydrogel is presented in **Figure 6**a, using the peripheral adipose tissue insulin transient and basal levels as the boundary and initial conditions for Equation (36), respectively, (data appear in Figure 5s), and the conversion for insulin concentration[45] $1\,\mathrm{mU\ L^{-1}} = 7.174\,\mathrm{pM}$).

The relative unbound site concentration according to Equation (37) was solved within the hydrogel, where the initial condition, g_{initial}, was calculated from Equations (24) and (25):

$$g_{\mathrm{initial}} = \frac{1}{\frac{C^h_{I\,\mathrm{initial}}}{K_d} + 1} \tag{41}$$

where $C^h_{I\mathrm{initial}}$ is the basal insulin concentration that was taken as the initial condition for Equation (36) as well. The relative bound insulin was calculated from the relative unbound sites. The concentrations of free and bound insulin within the hydrogel were then averaged over the gel thickness for each time point,

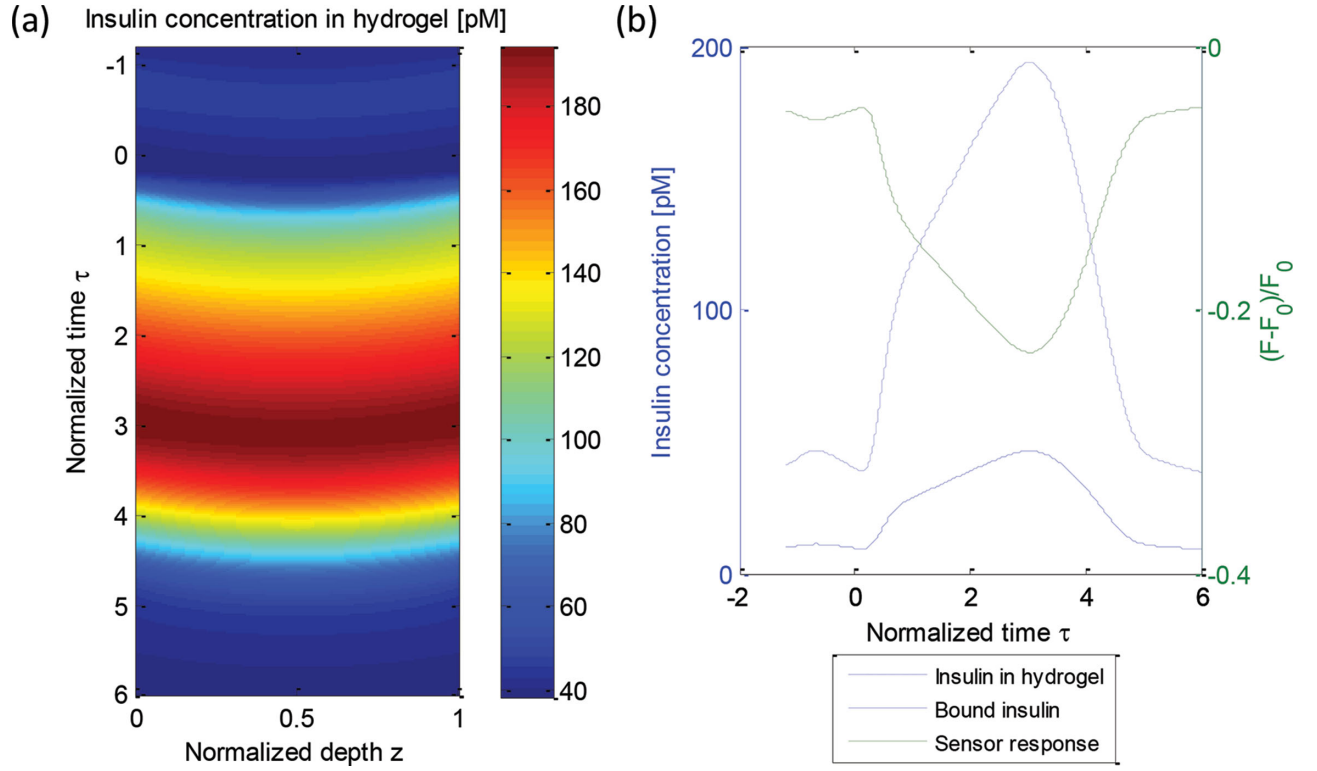

Figure 6. a) Insulin concentration within hydrogel encapsulating SWNT insulin sensors, implanted in the subcutaneous adipose tissue, for gel thickness of $L = 0.5$ mm, Thiele modulus $\phi = 50$, diffusion coefficient $D = 1 \times 10^{-6}$ cm^{2}s^{-1}, dissociation constant $K_d = 8.3$ μM, and rate constant $k = 1 \times 10^5$ M^{-1}s^{-1} following a 100 g glucose meal according to our model. b) Averaged insulin concentration within the hydrogel (dashed blue curve), averaged bound insulin concentration (blue curve), and sensor response (green curve).

and are plotted in Figure 6b as dashed and solid blue curves, respectively. The time lag between the bound insulin peak concentration and the free insulin peak concentration is 12 s, as expected from the short reaction time. The sensor response was calculated according to Equation (38), assuming an arbitrary proportion factor[21a] of $\beta = 1000$, and is plotted in Figure 6b (green curve). The maximum sensor response in this case is 23%. The time lag between the sensor response and the insulin concentration in tissue is approximately 4 min, resulting in a total time lag of 11 min between sensor response and plasma insulin concentration. Choosing a different proportion factor, β, would only affect the scale of the fluorescence response but would not change the shape of the sensor response curve or the sensor delay time.

3.3. Sensor Optimization

The parameters of the gel and of the insulin–sensor kinetics were varied one at a time, while keeping the others constant, in order to check their effect on both the sensor delay time relative to tissue concentration and the maximum response, which we wanted to minimize and maximize, respectively. First, we changed the gel thickness from 300 μm to 0.4 cm, keeping the dissociation constant, $K_d = 8.3$ μM, and the rate constant, $k = 1 \times 10^5$ M^{-1}s^{-1}, fixed (**Figure 7**a). As the gel thickness increased, the sensor delay increased from 1.5 to 27 min, and the sensor maximum response decreased from 23% to 12%. The Thiele modulus increases with the gel thickness squared. We can thus conclude that minimizing the gel thickness would be beneficial in terms of both of sensor delay time and the maximum response parameters, and for the following simulations we kept a minimal value of $L = 300$ μm.

The dissociation constant K_d was varied over three orders of magnitude ranging from 0.1 to 100 μM (Figure 7b). As the K_d value increased, the sensor delay time insignificantly increased from 1 to 5 min. However, the maximum sensor response significantly changed, increasing from 0.2% to 200%.

Finally, the rate constant k was varied over three orders of magnitude ranging from 10^3 to 10^6 M^{-1}s^{-1} (Figure 7c), where the Thiele modulus increased linearly with the rate constant. Although the maximum sensor response changed insignificantly from 22% to 23%, the sensor delay reduced from 14 to 1 min, as the rate constant increased.

The overall sensor delay can be shortened by using other implantation sites. The insulin concentration levels in the brain, heart and lungs, kidney, and gut compartments peak instantaneously with the peripheral vasculature concentration, whereas the liver insulin concentration is 4 min ahead and the peripheral interstitial insulin concentrations are delayed by 5 and 7 min for muscle and adipose tissue, respectively (Figure 5, panels (k)–(s)). All tissue delay times are small relative to the overall response time of the insulin concentration in the body following a meal, τ_{tissue}, which is of the order of 1 h.[46] Thus the implantation site can be chosen based on its accessibility for maximal external signal collection, which would favor the

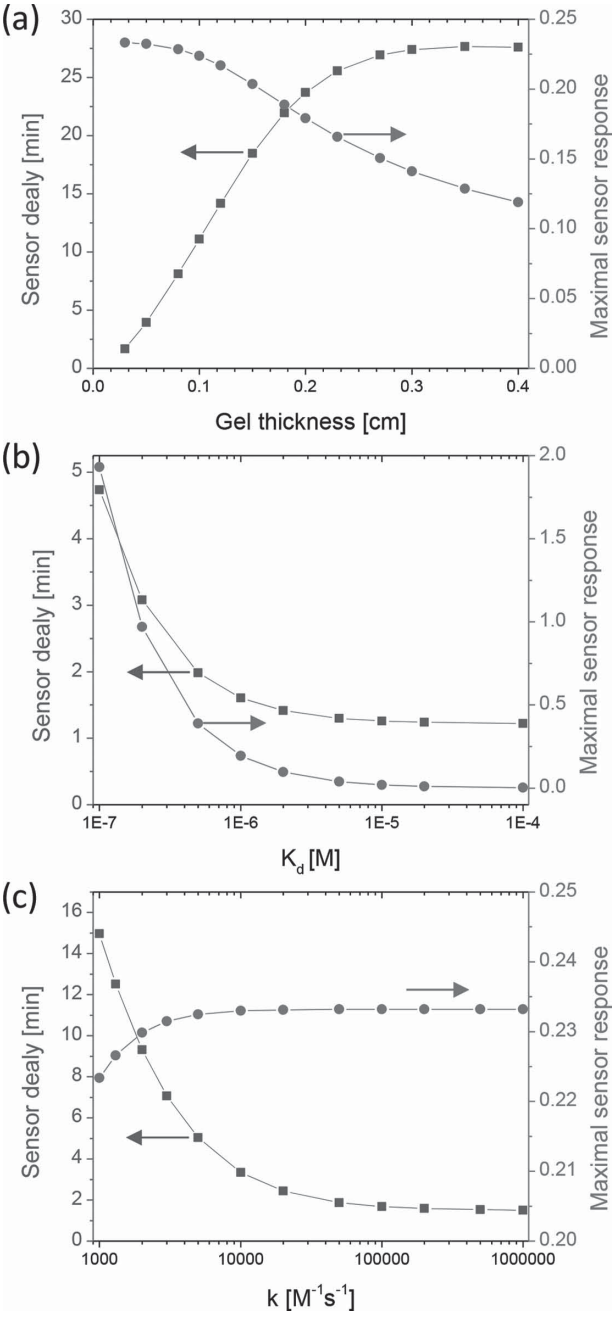

Figure 7. Insulin sensor delay time (blue curve) with respect to the surrounding tissue concentration and the maximum sensor response (green curve) as a function of a) the hydrogel thickness, b) the dissociation constant of the insulin–sensor reaction, and c) the rate constant of the insulin–sensor reaction, following a 100 g glucose meal according to our model. The arrows direct each curve to its corresponding y-axis.

subcutaneous space. However, given that future technologies allow for minimally invasive and efficient detection of near-infrared fluorescent probes in other tissue sites, our robust mathematical model can provide design and developmental information for all sensor in vivo locations.

In order to avoid the diffusion limitation of the sensor response, a gel must be thin enough to allow for rapid insulin diffusion. However, thinner hydrogel implants could lead to a lower single to noise ratio and would require highly efficient signal collection. Additional optimization can be achieved by utilizing a gradient thickness hydrogel that would satisfy the requirements of fast response along with high signal to noise ratio. Using the diffusion coefficient of insulin in aqueous solution[41] $D_a = 2.16\times10^{-6}\,\mathrm{cm^2 s^{-1}}$ as an upper bound for the diffusion within the hydrogel, the gel thickness must be less than 1 mm so that the characteristic diffusion time τ_D would be of the order of τ_{tissue} or less. Moreover, as long as the sensor kinetics are fast enough and $\tau_R \le \tau_D$, the sensor kinetics will not affect the time lag, and the sensor can be modeled as in equilibrium. For the maximal diffusion coefficient D_a, we would require $k \ge 10^3\,\mathrm{M^{-1}s^{-1}}$ and $k \ge 1.2\times10^4\,\mathrm{M^{-1}s^{-1}}$ for 1 mm and 300 μm gel thickness, respectively.

The total insulin binding site concentration, θ_T, can be manipulated by varying the concentration of sensors within the hydrogel. Given a particular SWNT-based sensor, other parameters such as the average nanotube length, and the linear density of insulin binding sites along the tube, are much more difficult to control and optimize in the synthesis process. An increase or a decreases of sensor concentration by a factor of 2, resulting in a similar change to the total insulin binding site concentration, does not change the maximum sensor response, and the sensor delay time remains the same within a range of 1 min.

4. Conclusion

We have derived a mathematical model of an insulin affinity sensor encapsulated within a biocompatible hydrogel suitable for implantation in the subcutaneous adipose tissue enabling external optical detection. A possible platform for the implementation of such a sensor is based on molecular recognition of the corona phase of SWNTs.[21a] The sensor response and delay time were calculated based on a full physiological model for insulin metabolism, which specifically included the adipose tissue, diffusion of the insulin into the hydrogel encapsulating the sensor, and the insulin–sensor interaction according to established models.[21a] For optimal sensor performance, the characteristic diffusion time should be less than the overall metabolism rate of the body in order to avoid diffusion limitations, and the characteristic insulin–sensor interaction time should be less than the diffusion time so the sensor can rapidly equilibrate and will have little additive effect on delay times.

Minimizing the gel thickness has the most profound effect on reducing the sensor delay time while moderately increasing sensor response. Furthermore, decreasing the dissociation constant has a dramatic effect on maximizing the sensor response, where its effect on the delay time is minimal. Finally, increasing the rate constant has a fair effect on decreasing the delay time but almost no effect on the sensor response.

Our model provides a principal basis for the design of an in vivo insulin affinity sensor, and would play a fundamental part in any experimental realization of such sensors. Our findings are essential for in vitro evaluation of an insulin sensor, providing objective criteria for sensor assessment and in vivo performance prediction.

Supporting Information

Supporting Information is available from the Wiley Online Library or from the author.

Acknowledgements

This research was supported by the Juvenile Diabetes Research Foundation. G. Bisker acknowledges the Technion-MIT postdoctoral fellowship, J. Ahn is grateful for the support of the Samsung scholarship, and N. M. Iverson thanks the National Institutes of Health T32 Training Grant in Environmental Toxicology ES007020.

Received: May 18, 2014
Revised: June 23, 2014
Published online: July 31, 2014

[1] A. Bascones-Martinez, P. Matesanz-Perez, M. Escribano-Bermejo, M. A. Gonzalez-Moles, J. Bascones-Ilundain, J. H. Meurman, *Med. Oral Patol Oral Cir. Bucal* **2011**, *16*, e722.
[2] a) C. Binder, T. Lauritzen, O. Faber, S. Pramming, *Diabetes Care* **1984**, *7*, 188; b) J. Li, Y. Kuang, *Math Biosci. Eng.* **2009**, *6*, 41.
[3] R. M. Bergenstal, W. V. Tamborlane, A. Ahmann, J. B. Buse, G. Dailey, S. N. Davis, C. Joyce, T. Peoples, B. A. Perkins, J. B. Welsh, S. M. Willi, M. A. Wood, *New Engl. J. Med.* **2010**, *363*, 311.
[4] C. M. Bennett, M. Guo, S. C. Dharmage, *Diabetic Med.* **2007**, *24*, 333.
[5] a) T. Battelino, I. Conget, B. Olsen, I. Schütz-Fuhrmann, E. Hommel, R. Hoogma, U. Schierloh, N. Sulli, J. Bolinder, *Diabetologia* **2012**, *55*, 3155; b) R. Gifford, *ChemPhysChem* **2013**, *14*, 2032.
[6] S. A. Weinzimer, G. M. Steil, K. L. Swan, J. Dziura, N. Kurtz, W. V. Tamborlane, *Diabetes Care* **2008**, *31*, 934.
[7] M. Laakso, *Am. J. Epidemiol.* **1993**, *137*, 959.
[8] a) R. A. DeFronzo, D. Simonson, E. Ferrannini, *Diabetologia* **1982**, *23*, 313; b) C. J. Greenbaum, *Diabetes Metab. Res. Rev.* **2002**, *18*, 192; c) E. Donga, M. van Dijk, R. P. Hoogma, E. P. Corssmit, J. A. Romijn, *Diabetes Metab Res. Rev.* **2013**, *29*, 33.
[9] S. E. Kahn, *Diabetologia* **2003**, *46*, 3.
[10] V. Singh, S. Krishnan, in *Meeting Abstracts*, The Electrochemical Society, **2013**, pp. 2657.
[11] a) R. S. Yalow, S. A. Berson, *J. Clin. Invest.* **1960**, *39*, 1157; b) J. D. M. Albano, R. P. Ekins, G. Maritz, R. C. Turner, *Acta Endocrinologica* **1972**, *70*, 487; c) S. Nakagawa, H. Nakayama, T. Sasaki, K. Yoshino, Y. Y. Yu, K. Shinozaki, S. Aoki, K. Mashimo, *Diabetes* **1973**, *22*, 590.
[12] M. J. MacDonald, J. P. Gapinski, *Metabolism* **1989**, *38*, 450.
[13] a) M. Xu, X. Luo, J. J. Davis, *Biosens. Bioelectron.* **2013**, *39*, 21; b) X. Luo, M. Xu, C. Freeman, T. James, J. J. Davis, *Anal. Chem.* **2013**, *85*, 4129.
[14] M. Frasconi, C. Tortolini, F. Botrè, F. Mazzei, *Anal. Chem.* **2010**, *82*, 7335.
[15] a) J. Wang, M. Musameh, *Anal. Chim. Acta* **2004**, *511*, 33; b) J. Wang, T. Tangkuaram, S. Loyprasert, T. Vazquez-Alvarez, W. Veerasai, P. Kanatharana, P. Thavarungkul, *Anal. Chim. Acta* **2007**, *581*, 1.
[16] A. Salimi, M. Roushani, S. Soltanian, R. Hallaj, *Anal. Chem.* **2007**, *79*, 7431.
[17] R. Schirhagl, U. Latif, D. Podlipna, H. Blumenstock, F. L. Dickert, *Anal. Chem.* **2012**, *84*, 3908.
[18] Y. M. Bae, B.-K. Oh, W. Lee, W. H. Lee, J.-W. Choi, *Biosens. Bioelectron.* **2004**, *20*, 895.
[19] Y. Pu, Z. Zhu, D. Han, H. Liu, J. Liu, J. Liao, K. Zhang, W. Tan, *Analyst* **2011**, *136*, 4138.
[20] J. Hilderink, C. Otto, C. Slump, A. Lenferink, M. Engelse, C. van Blitterswijk, E. de Koning, M. Karperien, A. van Apeldoorn, *PLoS One* **2013**, *8*, e78148.
[21] a) J. Zhang, M. P. Landry, P. W. Barone, J.-H. Kim, S. Lin, Z. W. Ulissi, D. Lin, B. Mu, A. A. Boghossian, A. J. Hilmer, A. Rwei, A. C. Hinckley, S. Kruss, M. A. Shandell, N. Nair, S. Blake, F. Sen, S. Sen, R. G. Croy, D. Li, K. Yum, J.-H. Ahn, H. Jin, D. A. Heller, J. M. Essigmann, D. Blankschtein, M. S. Strano, *Nat. Nano* **2013**, *8*, 959; b) S. Kruss, M. P. Landry, E. Vander Ende, B. M. A. Lima, N. F. Reuel, J. Zhang, J. Nelson, B. Mu, A. Hilmer, M. Strano, *J. Am. Chem. Soc.* **2013**, *136*, 713.
[22] a) S. Kruss, A. J. Hilmer, J. Zhang, N. F. Reuel, B. Mu, M. S. Strano, *Adv. Drug Delivery Rev.* **2013**, *65*, 1933; b) B. Mu, J. Zhang, T. P. McNicholas, N. F. Reuel, S. Kruss, M. S. Strano, *Acc. Chem. Res.* **2014**, *474*, 979.
[23] N. M. Iverson, P. W. Barone, M. Shandell, L. J. Trudel, S. Sen, F. Sen, V. Ivanov, E. Atolia, E. Farias, T. P. McNicholas, N. Reuel, N. M. A. Parry, G. N. Wogan, M. S. Strano, *Nat. Nano* **2013**, *8*, 873.
[24] S. M. Bachilo, M. S. Strano, C. Kittrell, R. H. Hauge, R. E. Smalley, R. B. Weisman, *Science* **2002**, *298*, 2361.
[25] a) P. W. Barone, S. Baik, D. A. Heller, M. S. Strano, *Nat. Mater.* **2005**, *4*, 86; b) Z. Liu, S. Tabakman, K. Welsher, H. Dai, *Nano Res.* **2009**, *2*, 85.
[26] M. J. O'Connell, S. M. Bachilo, C. B. Huffman, V. C. Moore, M. S. Strano, E. H. Haroz, K. L. Rialon, P. J. Boul, W. H. Noon, C. Kittrell, J. Ma, R. H. Hauge, R. B. Weisman, R. E. Smalley, *Science* **2002**, *297*, 593.
[27] S. Wray, M. Cope, D. T. Delpy, J. S. Wyatt, E. O. R. Reynolds, *Biochim. et Biophys. Acta (BBA) – Bioenergetics* **1988**, *933*, 184.
[28] P. W. Barone, R. S. Parker, M. S. Strano, *Anal. Chem.* **2005**, *77*, 7556.
[29] L. T. Nguyen, B. T. Lee, *Tissue Eng. Part A20* 13-14 1993 **2014**.
[30] J. S. Lee, J. Shin, H. M. Park, Y. G. Kim, B. G. Kim, J. W. Oh, S. W. Cho, *Biomacromolecules* **2014**, *15*, 206.
[31] P. L. Bollyky, R. B. Vernon, B. A. Falk, A. Preisinger, M. D. Gooden, G. T. Nepom, J. A. Gebe, *J. Diabetes Res.* **2013**, *2013*, 342479.
[32] D. E. Soranno, H. D. Lu, H. M. Weber, R. Rai, J. A. Burdick, *J. Biomed. Mater. Res. A102* 7 2173 **2014**.
[33] K. D. McKeon-Fischer, J. H. Rossmeisl, A. Whittington, J. W. Freeman, *Tissue Eng. Part A20* 13-14 1961 **2014**.
[34] E. Deat-Laine, V. Hoffart, G. Garrait, J. F. Jarrige, J. M. Cardot, M. Subirade, E. Beyssac, *Pharm. Res.* **2013**, *30*, 721.
[35] a) N. Alexandre, J. Ribeiro, A. Gartner, T. Pereira, I. Amorim, J. Fragoso, A. Lopes, J. Fernandes, E. Costa, A. Santos-Silva, J. D. Santos, A. C. Mauricio, A. L. Luis, *J. Biomed. Mater. Res. A* 2014, DOI: 10.1002/jbm.a.35098; b) T. Tokatlian, C. Cam, T. Segura, *Biomaterials* **2014**, *35*, 825.
[36] J. T. Sorensen, Ph.D. dissertation, Dept. of Chemical Engineering, Massachusetts Institute of Technology **1985**.
[37] a) K. Orcutt, K. Nasr, D. Whitehead, J. Frangioni, K. D. Wittrup, *Mol. Imaging Biol.* **2011**, *13*, 215; b) K. D. Orcutt, J. J. Rhoden, B. Ruiz-Yi, J. V. Frangioni, K. D. Wittrup, *Mol. Cancer Therapeutics* **2012**, *11*, 1365.
[38] W. W. Mapleson, *J. Appl. Physiol.* **1963**, *18*, 197.
[39] R. A. Jackson, N. Peters, U. Advani, G. Perry, J. Rogers, W. H. Brough, T. R. E. Pilkington, *Diabetes* **1973**, *22*, 442.
[40] E. D. Lehmann, T. Deutsch, *J. Biomed. Eng.* **1992**, *14*, 235.
[41] L. M. Weber, C. G. Lopez, K. S. Anseth, *J. Biomed. Mater. Res. Part A* **2009**, *90A*, 720.
[42] a) V. Thomé-Duret, G. Reach, M. N. Gangnerau, F. Lemonnier, J. C. Klein, Y. Zhang, Y. Hu, G. S. Wilson, *Anal. Chem.* **1996**, *68*, 3822; b) M. S. Boyne, D. M. Silver, J. Kaplan, C. D. Saudek, *Diabetes* **2003**, *52*, 2790; c) G. Velho, P. Froguel, D. R. Thevenot, G. Reach, *Biomed. Biochim. Acta* **1989**, *48*, 957.
[43] V. Sluzky, J. A. Tamada, A. M. Klibanov, R. Langer, *Proc. Natl. Acad. Sci.* **1991**, *88*, 9377.
[44] S. A. Berson, R. S. Yalow, *J. Clin. Invest.* **1959**, *38*, 1996.
[45] C. Colette, C. Percheron, N. Pares-Herbute, F. Michel, T. C. Pham, L. Brillant, B. Descomps, L. Monnier, *Int. J. Obes. Relat. Metab. Disord.* **2003**, *27*, 648.
[46] C. D. Man, R. A. Rizza, C. Cobelli, *Biomed. Eng., IEEE Trans.* **2007**, *54*, 1740.